Science and Technology Infusion Climate Bulletin
NOAA's National Weather Service
37th NOAA Annual Climate Diagnostics and Prediction Workshop
Fort Collins, CO, 22-25 October 2012

Is Global Warming Changing the ENSO Precursor in the Western North Pacific?

Shih-Yu Wang[1], Michelle L'Heureux[2], and Jin-Ho Yoon[3]

[1]*Utah Climate Center/Dept. Plants, Soils, and Climate, Utah State University, Logan, Utah*
[2]*NOAA Climate Prediction Center, College Park, Maryland*
[3]*Pacific Northwest National Laboratory, Richland, Washington*

1. Introduction

Recently, Wang *et al.* (2012) found that the boreal winter sea surface temperature anomalies (SSTA) in the western North Pacific (WNP) are strongly correlated to the development of the El Niño-Southern Oscillation (ENSO) by the following winter. Wang *et al.* (2012) defined the WNP index in two ways: (1) more simply by using de-trended SSTA averaged from 122°–132°E to 18°–28°N (a white box in Figure 1a) or (2) the second leading Maximum Covariance Analysis (MCA) of SSTA and 10m wind anomalies in the western Pacific from 90°E-170°W to 10°S-30°N (Figure 1a). In this study, the WNP will refer to the combined pattern of anomalous SST and winds, which is analogous to the Pacific Meridional Mode (PMM) located in the eastern half of the North Pacific. Both the PMM and WNP are linked to an SSTA dipole with significant anomalies off the equator in the Northern Hemisphere subtropics with opposing SSTAs located in the deep tropics. The PMM and WNP are thought to be linked to the "Seasonal Footprinting Mechanism (SFM)" (Vimont *et al.* 2003a,b; Alexander *et al.* 2010), when the atmospheric circulation over the extratropical North Pacific during the boreal winter (linked to the North Pacific Oscillation/NPO) establishes an SSTA pattern that persists through the following year and eventually influences ENSO. Wang *et al.* (2012) suggested that the location of the WNP SSTA dipole and associated wind anomalies (Figure 1a) may exert a more direct influence than the PMM on the degree of oceanic Kelvin wave activity preceding ENSO events (McPhaden 2004; Roundy and Kiladis 2007).

Here we report new observational and modeling evidence that, since the mid-20th century, there is a growing association between the WNP and the development of ENSO by the following year. The stronger relationship between the WNP and ENSO appears to be linked to increased greenhouse gas (GHG) in the atmosphere, and it may reflect the energetic west-to-east development of ENSO in recent decades (Wang and An 2002; Guan and Nigam 2008). Furthermore, a greater link between the WNP and ENSO one year later provides a plausible pathway by which anthropogenic climate change may influence ENSO and perhaps provide greater predictive skill in seasonal ENSO outlooks.

2. Data sources

To mitigate potential errors in historical SST data and reanalysis methods, three monthly SST datasets are utilized: (1) the Hadley Centre SST (HadISST) (Rayner *et al.* 2003), (2) the NOAA Extended Reconstructed SST (ERSST) Version 3b (Smith *et al.* 2008), and (3) the Kaplan long-term SST anomalies (Kaplan *et al.* 1998). Atmospheric winds are obtained from the NCEP/NCAR Global Reanalysis (NCEP1) that begins in 1948 (Kalnay *et al.* 1996). In addition, to examine the long-term changes in the WNP and ENSO, historical simulations with the Community Earth System Model version 1 (CESM1) are analyzed. Deser *et al.* (2011) showed the Community Climate System Model (CCSM4) – predecessor of the CESM1 but sharing the same ocean model – demonstrates significantly improved ENSO variability. This study uses three CMIP5 sets of historical single-forcing experiments that are driven by (a) greenhouse gas forcing only (GHG), (b) aerosol forcing only (Aerosol), and (c) natural forcing only including solar and volcano (Natural). Each experiment produced a two-member ensemble initialized from long-stable preindustrial (1850) control

Correspondence to: Shih-Yu Wang, Utah Climate Center/Dept. Plants, Soils, and Climate, Utah State University, Logan, Utah; E-mail: simon.wang@usu.edu.

runs up to 2005. In addition, we utilize a 350-year fully coupled CESM1 simulation without any external forcings. This long-term control simulation is useful to depict the natural variability of the WNP and ENSO.

3. Results

a. Strengthening of the WNP (DJF) and ENSO (DJF+1yr) association

Throughout this analysis, the WNP index is based on the second leading MCA mode of the western North Pacific SSTA and anomalous surface winds, but the major findings are also reproduced using an index of the box average SSTA. In order to align with above-average anomalies associated with the WNP box average, the positive phase of the MCA/WNP is defined by the anomalous pattern of SST and winds shown in Figure 1a. Figure 1b shows the 25-year sliding correlation between the WNP index during boreal winter (December-February, DJF) and the Niño-3.4 index (average SSTA for 170°-120°W, 5°S-5°N) during the following winter (DJF+1yr). The x-axis corresponds to the final year of the correlation window. A strong increase in correlations between the WNP and ENSO (DJF+1yr) is evident among all three SST datasets (Figure 1b). Here, the WNP and Niño-3.4 indices are linearly de-trended within each 25-year moving window in order to examine the interannual correlations between the WNP and ENSO irrespective of multi-decadal or longer trends. We note that either removing a single, fixed trend over the entire analysis period or keeping the trend results in similar increases in the correlation with a difference less than 0.1 (not shown). This increase is particularly robust for moving windows that begin with 1960 as the initial year.

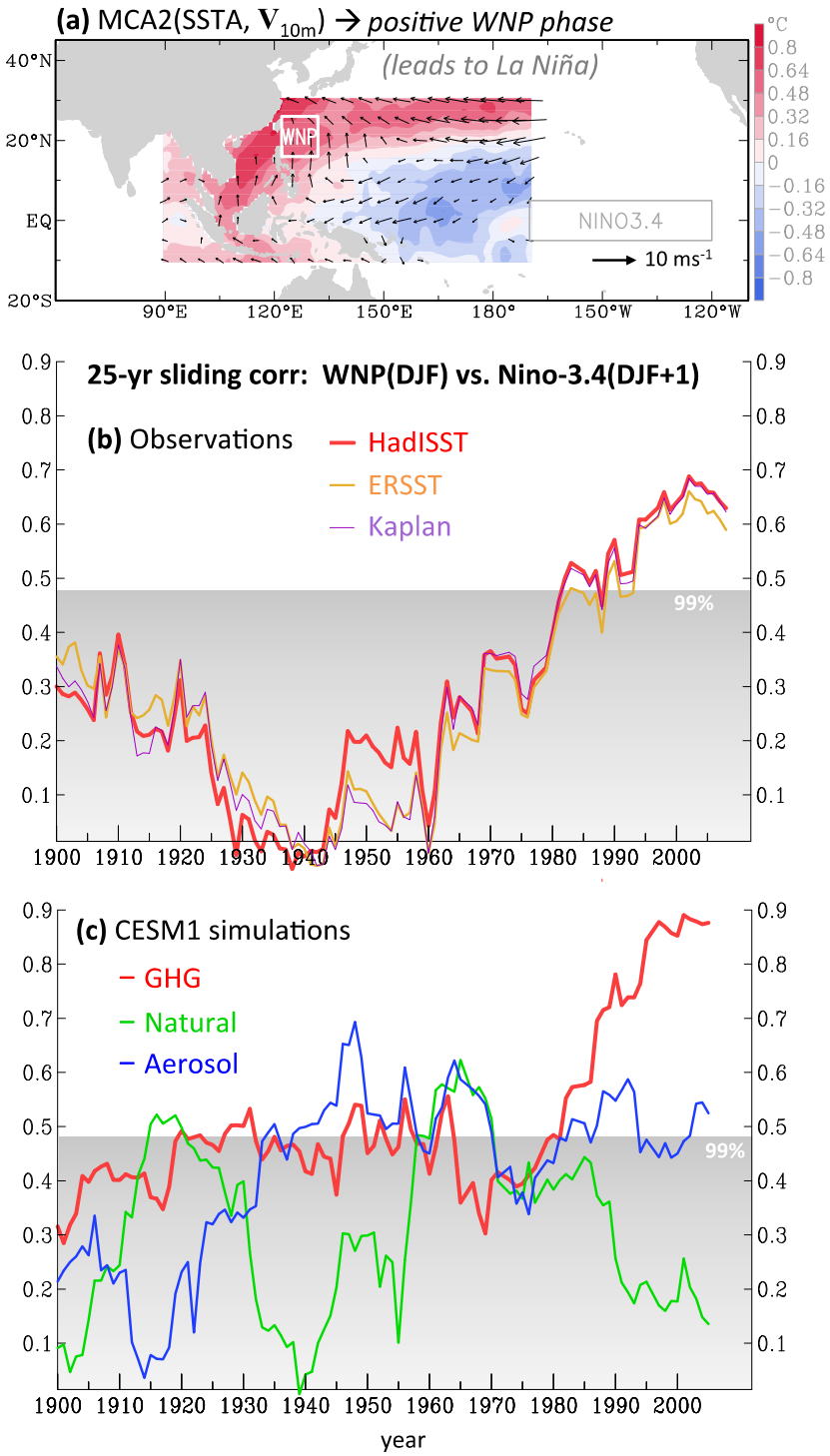

Fig. 1 (a) MCA-2 of WNP SSTA and surface wind anomalies in DJF, adopted from Wang et al. (2012). The PC time series of MCA2 is used as the WNP index. Outlined areas represent an alternative WNP index domain and the Niño-3.4 index domain. (b) 25-year sliding correlations betwenn the WNP (DJF) and Niño-3.4 (DJF+1yr) indices using three SST datasets. Years on the x-axis represent the final year of the 25-year sliding window. The top of gray area indicates the 99% significance level. (c) Same as (b) but for the three CESM1 experiments.

The correlation has increased to as high as 0.7 in the most recent part of the record. This result is robust regardless of the length of the sliding windows (not shown).

Figure 2a shows one-point correlation maps between SSTA and the WNP index at lead times of zero-year (left) and one-year (right), using HadISST data for the period 1958-2010 (Wang *et al.* 2012). The WNP index is inverted, so the map can be interpreted as the negative WNP phase that precedes El Niño. During DJF, strong correlations are evident along the East Asian coastline and along the Kuroshio Extension. In the following winter (DJF+1yr), the WNP is related to a significant basin-wide El Niño SSTA pattern.

The WNP-ENSO association is examined using CESM1 simulations forced by the GHG, Natural, and Aerosol forcings to understand the role of external forcings (Figures 2b-2d). The correlations between the WNP and SSTA based on the forcing experiments for DJF (left) and DJF+1yr (right) during 1958-2005 bear a strong resemblance with the observations. Key aspects of the WNP relationship with SSTA are broadly reproduced, with the exception of opposing correlations in the eastern Indian Ocean. Furthermore, Figure 1c shows 25-year sliding correlations between de-trended values of the WNP (DJF) and Niño-3.4 indices one year later (DJF+1yr) for the three CESM1 single forcing experiments. A considerable amount of decadal variability of the correlation between the WNP and ENSO is observed among the forcing experiments. While the Aerosol and Natural forcing experiments show significant correlations between the WNP and ENSO for periods between ~1940/50 through 1960/70, only the GHG forcing provides evidence for strong increase in

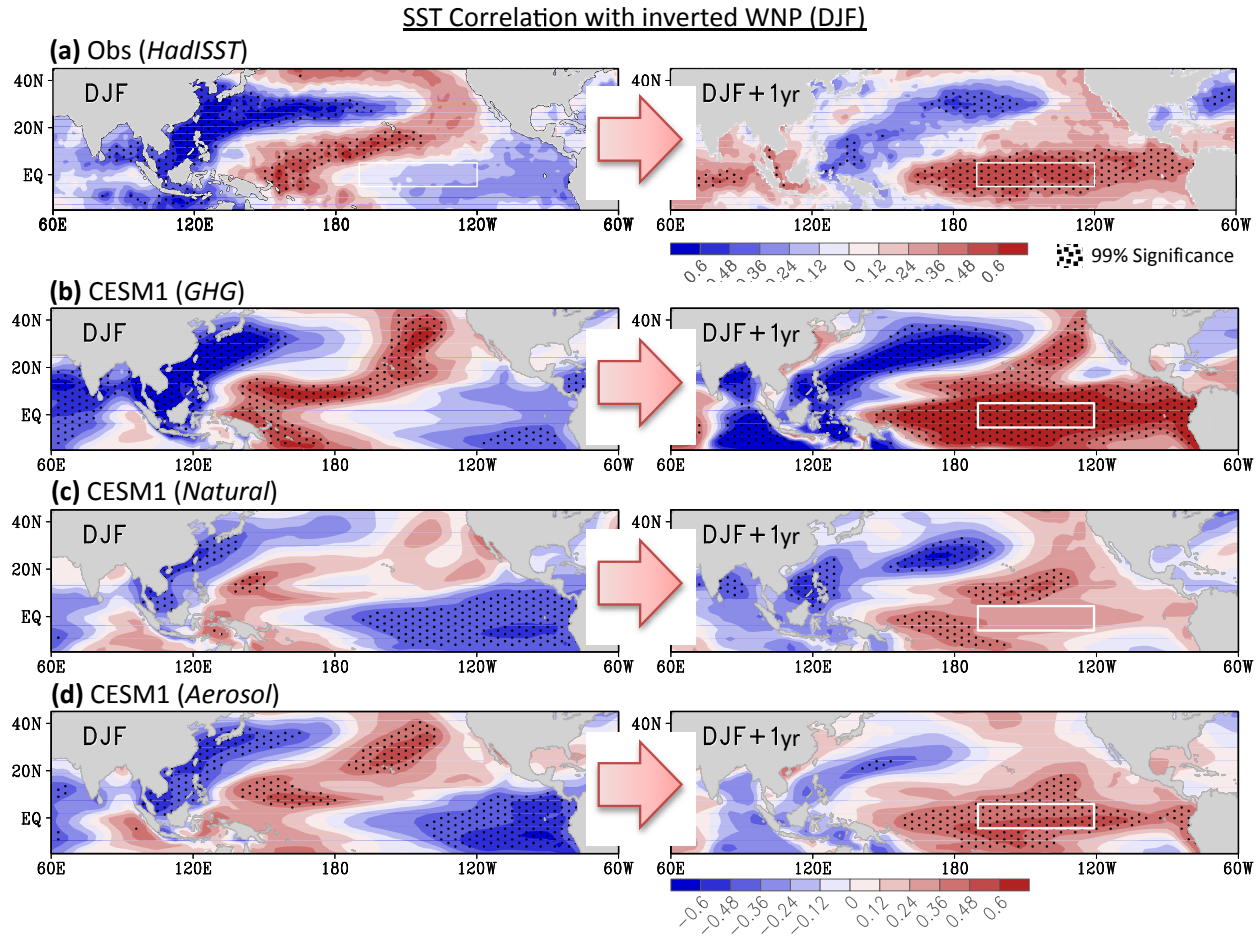

Fig. 2 (a) Corelation maps of SSTA with the inverted WNP index for zero-lead DJF (left) and one-year lead, DJF+1yr (right) using the HadISST and NCEP1 data for the period 1958-2010. All variables are detrended. The Niño-3.4 area is outlined. Dotted values are significance at the 99% level per a t-test. (b)-(d) Same as (a) but for the CESM1 simulations from the GHG, Natural, and Aerosol forcing experiments for the period 1958-2005.

the correlations that begins during ~1950-1970 and continues through the present. The GHG-only experiment indicates correlations as strong as ~0.9 between the WNP (DJF) and ENSO (DJF+1yr) in the recent decade while the Natural-only experiment indicates an insignificant relationship. Because these experiments are free runs, the specific years among the model experiments cannot be directed compared. Thus, the only robust comparison in Figure 1c is that neither the Aerosol-only run nor the Natural-only run produces a sustained period of significant correlations as large, or for long, as the GHG-only experiment.

b. Shifts in the strongest SST trends and the WNP (DJF) - ENSO (DJF+1yr) association

To better understand why the de-trended, interannual relationship between the WNP (DJF) and ENSO (DJF+1yr) has increased, we split the dataset into two halves: 1950-1979 and 1980-2008. The year 1950 is chosen as a starting point due to greater reliability in the observed datasets over the tropical Pacific after that time (Bunge and Clarke 2009; L'Heureux *et al.* 2012). To further suppress sampling errors, two SST datasets (HadISST and ERSST) are averaged together. Figures 3a and 3b show the SSTA correlations and the low-level wind regressions in DJF with the DJF+1yr Niño-3.4 index (the length of the vectors are weighted by the correlation). Comparing the two halves, the most striking and pronouced change in the recent era is the stronger regression/correlation between ENSO (DJF+1yr) and the previous DJF low-level wind anomalies curling southward and then eastward in the western equatorial Pacific just north of Papua New Guinea. Also evident is a stronger out-of-phase SSTA correlation between the subtropical western North Pacific and western equatorial Pacific (~160°E-180°). This result mirrors the inverse of Figure 1a and strongly implies that one of the canonical initiating mechanisms for ENSO onset has become more active recently: namely, the generation of oceanic Kelvin waves by wind stress anomalies over the western equatorial Pacific.

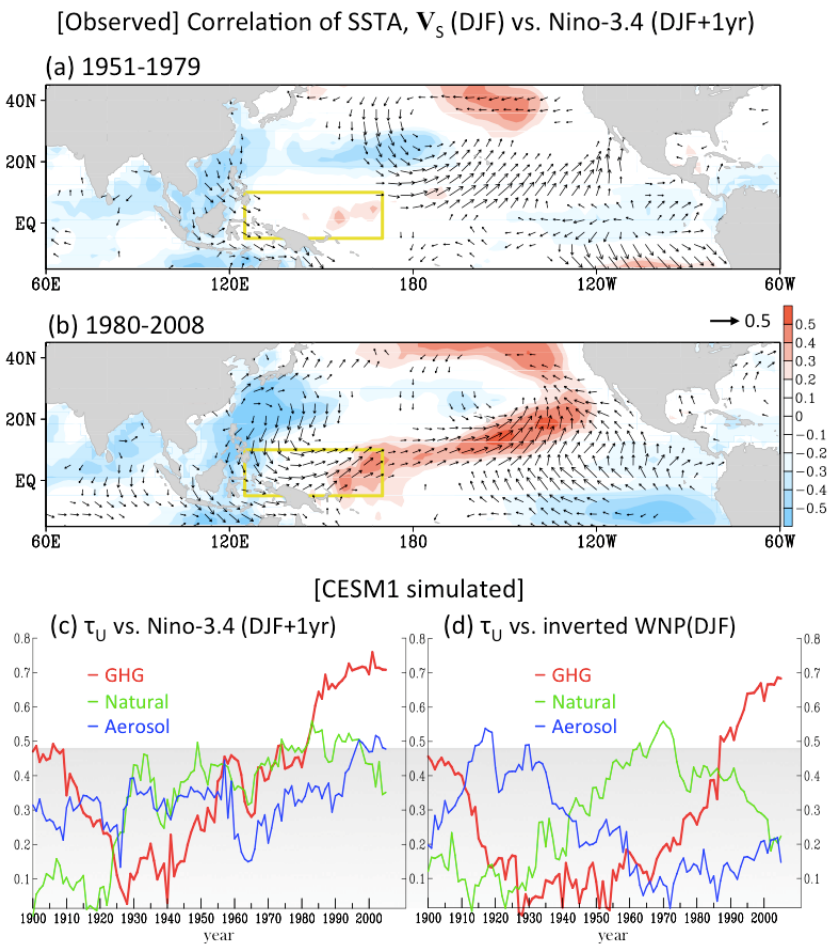

Fig. 3 Correlation map of DJF SSTA (shadings) and regression of surface winds weighted by the correlation (vector length) against the DJF+1yr Niño-3.4 index during the periods of (a) 1951-1979 and (b) 1980-2008, using the NCP1 wind and averaged HadISST-ERSST data. The plotted values exceed significance at the 95% level. (c) Similar to the 25-year sliding correction in Fig. 1b and 1c, but for the DJF surface wind stress (τ_U) (averaged in the yellow box in a, b) and the DJF+1yr Niño-3.4 index from the three CESM1 experiments. (d) Same as (c) except for correlations between τ_U and the inverted DJF WNP index.

Given that low-level wind anomalies in the western equatorial Pacific are optimally situated to influence the generation of oceanic Kelvin waves that affect the development of ENSO, we show in Figures 3c and 3d the CESM1 25-year sliding correlations of the de-trended surface zonal wind stress averaged for 120°-170°E, 5°S-10°N (τ_U) with the de-trended Niño-3.4 (DJF+1yr) and WNP (DJF), respectively. Among all the forcings, only the GHG-only forcing illustrates the pronounced upward correlation of low-level wind stress in the

equatorial western Pacific and the WNP with ENSO beginning in the mid-20th century. The increased correlations of the low-level winds provide more evidence for a GHG-driven increasing relationship between the WNP and ENSO development by the following year.

c. The changing ENSO precursor pattern

Why are there stronger correlations of the low-level winds in the western tropical Pacific and the WNP (DJF) with ENSO (DJF+1yr) index in the recent decades? To further examine the extent of which the low-level wind fields may change the ENSO-WNP link, Figure 4 presents composites of DJF SSTA and winds one year prior to El Niño in (a) and La Niña in (b), using a ±0.5°C threshold in the DJF Niño-3.4 index. The composite differences between the two eras, which are not de-trended, emphasize the change in the preceding SSTA and winds from the earlier period to the most recent period. The bottom panel is the difference between the top (a) and middle (b) panels and demonstrates how the differences between El Niño and La Niña preconditions are changed in the recent era and, as expected, largely replicate the ENSO correlations shown in Figure 3b. Unlike the correlations in Figure 3, this composite stratification allows for an examination of how the precursor SSTs have changed for El Niño and for La Niña separately. Interestingly, a comparison between Figures 4a and 4b reveals that positive SST trends east of Taiwan/south of Japan are greater prior to La Niña whereas these positive trends are relatively muted prior to El Niño. On the equatorial Western Pacific, positive SST trends are stronger prior to El Niño (~160°E-180) relative to those prior to La Niña. The differences (Figure 4c) mirror the correlations (Figure 3b) with both depicting a SSTA dipole and strong curvature of the winds connecting the subtropical WNP to the equator. Thus, it appears SST trends prior to ENSO events have changed location with relatively greater amplitudes collocated with the positive anomalies in the WNP dipole. This sharpening of the positive SST anomalies appears to arise in a strengthened WNP-ENSO relationship in the interannual timescales. However, why the GHG-associated SST trends vary between El Niño and La Niña in a manner that more strongly amplifies the above-average regions of the WNP dipole is unclear.

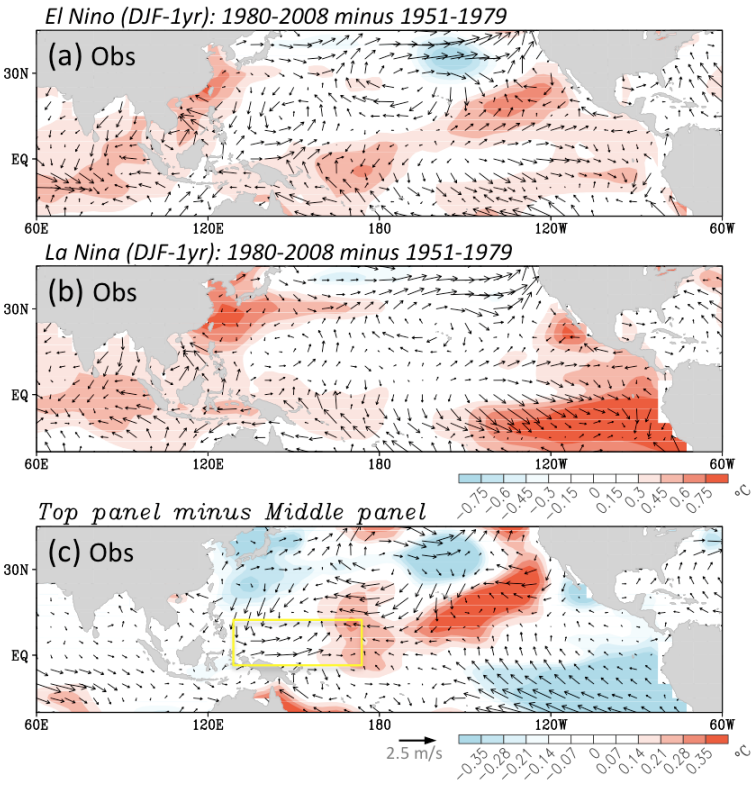

Fig. 4 Composite differences of SSTA (shading) and surface wind (vector) prior to (a) El Niño (DJF-1yr) and (b) La Niña (DJF-1yr) between the two eras of 1951-1979 and 1980-2008. (c) Differences between (a) and (b). The wind fields are averaged from 20CR and NCEP1 while the SSTA fields are averaged from HadlSST and ERSST.

4. Summary

While the WNP index is significantly correlated to the development of ENSO by the following winter, the analysis presented here further suggests that this relationship between the WNP and ENSO has significantly increased since the mid-20th century. The stronger WNP-ENSO association occurs on interannual timescales based upon de-trended data, so is not the direct result of the SST warming trends. CESM1 single forcing experiments suggest that the increased relationship is forced by increasing GHG in the atmosphere. The recent era is characterized by strengthening of the low-level wind anomalies in the equatorial western Pacific one year prior to ENSO, and an AMIP-style run implies this strengthening is due to shifts in the location of positive SST trends relative to El Niño or La Niña (one year previously). Prior to El Niño, the

region of positive SST trends occurs near the typical region of above-average SSTA in the western equatorial Pacific, whereas prior to La Niña, positive SST trends reinforce the above-average SSTA near southeastern Asia.

It is hypothesized that this shift in SST trends, which sharpens and amplifies the above-average SST region of the WNP dipole, arises in a strengthening WNP-ENSO relationship on interannual timescales. Analysis of the 350-year CESM1 preindustrial control simulation reveals that fluctuations in the leading North Pacific SSTA pattern of multi-decadal (30-year) variability mirror the variability in the correlations between the WNP and ENSO. While the control simulation only reflects coupled climate variability without external forcings, CESM1 suggests anthropogenic forcings, particularly GHG, have facilitated and even accelerated such a WNP-ENSO relationship. In recent decades, both the GHG-forcing experiment and the observations indicate unprecedented correlations closer to 0.7-0.9 between WNP and ENSO the following winter.

These results provide an important example of how lower frequency changes, like anthropogenic climate change, can directly impact intraseasonal-to-interannual climate variations. Provided that prediction tools can adequately capture the WNP-ENSO connection, if GHG are increasing the WNP-ENSO relationship then this may suggest potentially more skillful ENSO forecasts at one-year lead and increased confidence in seasonal predictions during the decades to come.

References

Alexander, M. A., D. J. Vimont, P. Chang, and J. D. Scott, 2010: The Impact of Extratropical Atmospheric Variability on ENSO: Testing the Seasonal Footprinting Mechanism Using Coupled Model Experiments. *J. Climate*, **23,** 2885-2901.

Bunge, L., and A. J. Clarke, 2009: A Verified Estimation of the El Niño Index Niño-3.4 since 1877. *J. Climate*, **22,** 3979-3992.

Deser, C., and Coauthors, 2011: ENSO and Pacific Decadal Variability in the Community Climate System Model Version 4. *J. Climate*, **25,** 2622-2651.

Guan, B., and S. Nigam, 2008: Pacific Sea Surface Temperatures in the Twentieth Century: An Evolution-Centric Analysis of Variability and Trend. *J. Climate*, **21,** 2790-2809.

Kalnay and Co-authors, 1996: The NCEP/NCAR 40-year reanalysis project. Bull. Amer. Meteor. Soc., 77, 437–470.

Kaplan, A., M. Cane, Y. Kushnir, A. Clement, M. Blumenthal, and B. Rajagopalan, 1998: Analyses of global sea surface temperature 1856-1991. *J. Geophys. Res*., **103,** 18567-18589.

L'Heureux, M. L., D. C. Collins, and Z.-Z. Hu, 2012: Linear trends in sea surface temperature of the tropical Pacific Ocean and implications for the El Nino-Southern Oscillation. *Clim. Dynamics***,** 1-14.

McPhaden, M. J., 2004: Evolution of the 2002/03 El Niño. *Bull. Amer. Meteor. Soc*., **85,** 677-695.

Rayner, N. A., and Coauthors, 2003: Global analyses of sea surface temperature, sea ice, and night marine air temperature since the late nineteenth century. *J. Geophys. Res*., **108,** 4407.

Roundy, P. E., and G. N. Kiladis, 2007: Analysis of a Reconstructed Oceanic Kelvin Wave Dynamic Height Dataset for the Period 1974,Äì2005. *J. Climate*, **20,** 4341-4355.

Smith, T. M., R. W. Reynolds, T. C. Peterson, and J. Lawrimore, 2008: Improvements to NOAA's Historical Merged Land–Ocean Surface Temperature Analysis (1880–2006). *J. Climate*, **21,** 2283-2296.

Vimont, D. J., D. S. Battisti, and A. C. Hirst, 2003b: The Seasonal Footprinting Mechanism in the CSIRO General Circulation Models. *J. Climate*, **16,** 2653-2667.

Vimont, D. J., J. M. Wallace, and D. S. Battisti, 2003a: The Seasonal Footprinting Mechanism in the Pacific: Implications for ENSO. *J. Climate*, **16,** 2668-2675.

Wang, B. W., and S. A. An, 2002: A mechanism for decadal changes of ENSO behavior: roles of background wind changes. *Clim. Dynamics*, **18,** 475-486.

Wang, S.-Y., M. L'Heureux, and H.-H. Chia, 2012: ENSO prediction one year in advance using western North Pacific sea surface temperatures. *Geophys. Res. Lett.*, **39,** L05702.